11th World Congress on Computational Mechanics (WCCM XI)
5th European Conference on Computational Mechanics (ECCM V)
6th European Conference on Computational Fluid Dynamics (ECFD VI)
E. Oñate, J. Oliver and A. Huerta (Eds)

USAGE OF REDUCED NUMERICAL MODELS IN THE DESIGN PROCESS OF A SHUNTED PIEZOELECTRIC ISOLATOR

TORSTEN BARTEL[*], OLIVER HEUSS[*], TOBIAS MELZ[*], FRANCISCO SCINOCCA[†], AIRTON NABARRETE[†] AND LUIZ C. S. GOES[†]

[*] Fraunhofer Institute for Structural Durability and System Reliability (LBF)
Darmstadt, Germany
e-mail: torsten.bartel@lbf.fraunhofer.de, www.lbf.fraunhofer.de

[†]Instituto Tecnológico de Aeronáutica (ITA)
São José dos Campos, SP, Brazil
www.ita.br

Key Words: *Smart Material, Vibration Isolation, semi-passive Systems, Modal Synthesis*

Abstract. This paper presents the design process and measurement results of a shunted piezoelectric isolator, which can be a good compromise between a solely passive and an active isolator. The system will be used for the reduction of the vibration transmission between two idealized panels of a plane fuselage. During the design process, numerical models of both, the panel structure and the shunted isolator, are used in order to derive reduced state-space matrices. Based on modal superposition, the numerical models describe the dynamic behaviour of the components and are integrated into a simulation environment of the holistic system. The required modal data is derived from experimental and numerical modal analyses of the panel. By means of an analytical description, the geometry of the shunted piezoelectric isolator is automatically optimized to defined goal parameters. Applying an impedance-admittance simulation approach, both the isolator and the shunt circuit are modeled. Using this simulation environment, the configuration and the performance of the shunt can be investigated and adjusted. After hardware realization of the shunted isolator, it is examined in a test setup. The results from test measurements are compared to simulation results of the system. Finally, two shunted isolators are placed between a fuselage panel and an ideal mass. Measurement results show the vibration reduction potential of the semi-passive system in addition to the solely passive isolation effect. This paper indicates the feasibility of shunted piezoelectric elements in addition to the passive isolation system. Furthermore an effective preliminary design strategy for the layout of shunted piezoelectric isolators is presented and compared to measurement results.

1 INTRODUCTION

The design of modern technical systems is highly affected by the increase of performance and by the usage of lightweight methods, while there are higher restrictions and demands on noise and vibration levels. In more and more applications, these contrary requirements cannot

be countered by solely passive measures. In this case, systems for active vibration reduction are used under the restriction of the necessity of a power supply [7]. However, using these systems, a significant improvement of the relationship between weight and power can be achieved, thus gaining an advantage in lightweight structure, such as aircraft [12] or satellite applications [5]. In between the fields of passive and active vibration reduction, there are semi-passive systems. Such systems can increase the performance of passive measures without the need for an external power supply [16]. One approach for a semi-passive system is the shunt damping technique associated with piezoelectric materials [9].

The present paper is focused on the vibration reduction using the shunt damping technique in combination with a vibration isolator for reducing the vibration transmission of a typical aeronautical panel, normally applied to aircrafts. The aim of this work is the reduction of the vibration transmissibility between the outer panel of the aircraft and its interior.

1.1 **Active, passive and shunted vibration isolation**

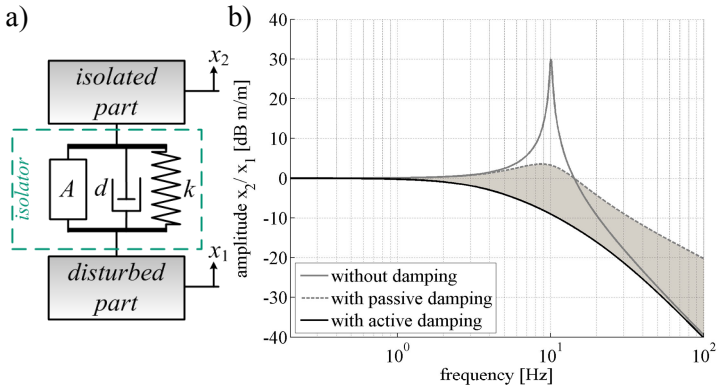

Figure 1: Transmissibility curves of an isolation system for passive and active vibration isolation
a) Scheme of an isolation system
b) Active and passive isolation curve

The scheme of an isolation system is depicted in Figure 1(a). A mechanical vibration isolator, located between the disturbed part and the isolated structure has the stiffness *k*, the damping *d* and, if required, an actuator A. A typical displacement response for an isolated part related to a disturbed part is showed in Figure 1(b) for active and passive isolation systems. As shown, the undamped isolator effects an increasing vibration isolation of -40 dB per decade in the frequency range above the resonance of the mass-spring system. An arising drawback is the vibration amplification in the region around the resonance frequency. The amplification can be reduced by adding a passive damper which however also reduces the isolation effect at higher frequencies. In addition, the active isolation unites the advantages of damped and undamped systems, as can also be seen in Figure 1(b). While the broadband isolation remains at frequencies above the resonance, the vibration amplification in the region around the resonance frequency can be reduced representing the effect of a mechanical damping element [15].

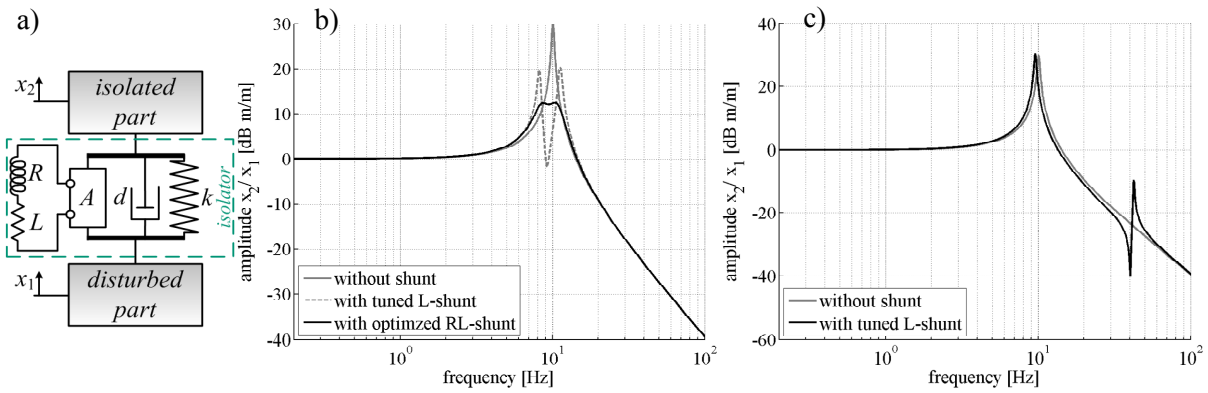

Figure 2: Transmissibility curves of a shunted isolation system
a) Scheme of an shunted isolation system
b) Damped absorption of the resonance amplification
c) Neutralization of a single harmonic excitation

Besides all advantages, the requirement of power amplifiers for the actuators is a negative aspect of active isolation systems, making them unfeasible for certain applications. A compromise between passive and active isolation can be the integration of a shunted electric circuit as described in [9], i.e. a shunted electromagnetic transducer [6]. The characteristics of an RL-shunted piezoelectric isolator is shown in Figure 2(a).

Two possibilities to adjust an RL-shunt are based on the absorption of the resonance amplification and on the neutralization of a single harmonic excitation as shown in Figure 2(b) and Figure 2(c), respectively. By tuning and optimizing the RL-shunt, an effect similar to a damped vibration absorber is achieved. Thus the resonance amplification can be reduced without a loss of isolation at higher frequencies. The tuning of the shunt to a higher frequency enables the neutralization of a single harmonic excitation. Since the shunt causes additional resonance amplification, the neutralization effect is less suitable for broadband excited systems.

1.2 Integration of a shunted isolator into a plane fuselage demonstration setup

The integration of a passive spring-damper element into the transmission path is the state of the art in order to achieve vibration isolation between two panels of a plane fuselage [11].

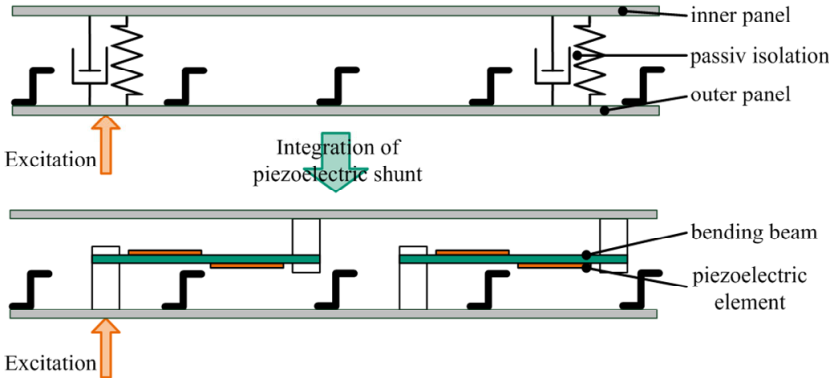

Figure 3: Concept of the integration of a shunted isolator to an airplane fuselage

In this work, these passive elements are substituted by a shunted piezoelectric bending beam as presented in Figure 3. A specific aim is to prove the feasibility principle of a shunted piezoelectric isolator.

Based on the published measurement data of a specific airplane (i.e. [13]), an idealized but realistic excitation scenario for the outer fuselage structure is assumed. This excitation scenario consists of a harmonic excitation force including harmonics promoted by the jet engine and a broad banded random force excitation caused by the air flow. The harmonic excitation is defined to be 50 Hz (3000 rpm), while the random excitation is broadband from 40 Hz to 160 Hz.

2 MODAL ANALYSIS OF THE AIRCRAFT PANEL

According to Figure 4(a), an idealized flat panel, similar to those normally applied in the aeronautical industry, is set up in order to conduct the investigation on the effectiveness of the shunted isolator. An experimental modal analysis is performed to analyze the dynamic behavior of the panel structure and the results are compared with that of a numerical model analysis. For a reasonable definition of the global and local modes in the area between stiffeners, 253 distinct measurement points are chosen.

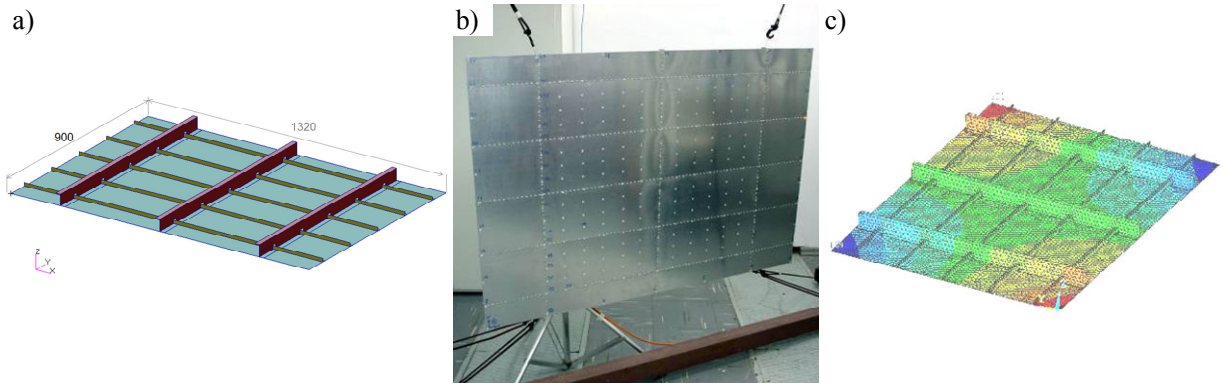

Figure 4: Measurement setup for modal analyses
a) Setup of the aircraft panel demonstrator
b) Measurement points at the front side of the aircraft panel
c) Finite-Element model of the aircraft panel

Figure 4(b) shows the reflection points that define the measurement grid. In order to measure the dynamic response curves, an electrodynamic shaker for excitation and a laser vibrometer system is used. The according finite element model is depicted in Figure 4(c). Figure 5 gives an exemplary comparison of investigated characteristic mode shapes. The first bending mode occurs at 27 Hz, as showed on Figure 5(a.1). In this frequency range the plate behaves similar to a conventional flat panel in free-free condition. In the mode shape shown in Figure 5(a.2), the bending of the stiffeners is dominant. Figure 5(a.3) illustrates the mode shape, in which local deflections of the single plate-elements between the stiffeners are recognizable. The latter type will also appear at higher frequencies on the real fuselage panel. Figure 5(b.1, b.2, b.3) shows the same mode shapes calculated by a numerical modal analysis.

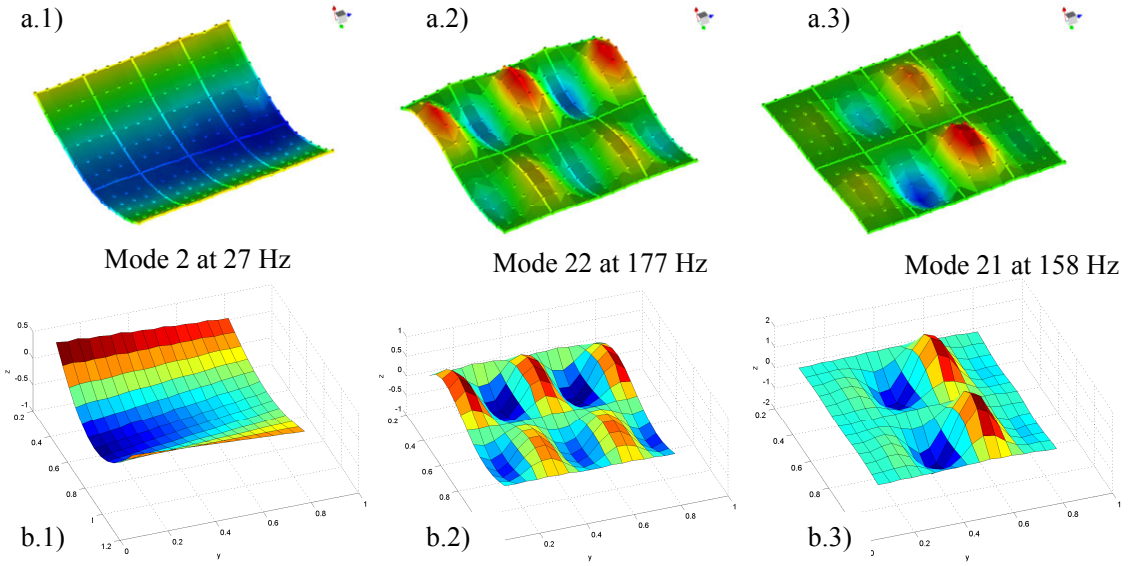

Figure 5: Characteristic mode shapes.
a) Experimental estimated mode shape: Global shape (a.1), Stiffener-dominated shape (a.2), Plate-element-dominated shape (a.3).
b) Correspondent numerical estimated mode shapes (b.1, b.2, b.3)

3 MODELLING AND SIMULATION OF THE SHUNTED SYSTEM

This chapter gives an overview of the used admittance-impedance modeling principle. After the description of the design and the optimization of the shunted isolator, the integration of both the isolator and the base structure into the simulation environment is given.

3.1 Principle of the admittance-impedance formulation of a mechanical system

Following the admittance-impedance approach [10], the electrical and the mechanical components are described in an analog way.

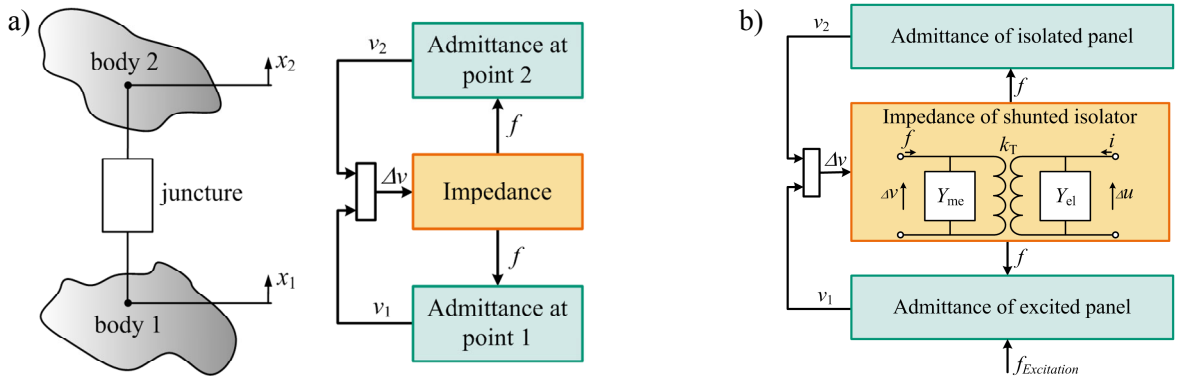

Figure 6: Principle of the mechanical admittance-impedance approach
a) Principle setup
b) Modeling scheme of a shunted system

While for electrical components this approach is very common, the electromechanical analogies are used for the formulation of the mechanical simulation part. Therefore the

disturbed and mounted bodies are expressed as admittances, while the juncture elements correspond to impedances as shown in Figure 6(a). Internal forces, caused by the impedances, and external forces are inputs to the admittances. The output is the resulting velocity of the body. The inputs to the impedances are the differences in velocities of the adjoined bodies. The outputs are the resulting forces. The derived model of the panel with the shunted isolator is depicted in Figure 6(b).

3.2 **Setup of the simulation model**

The simulation model consists of three different parts which are the fuselage panel as the excited body, the shunted isolator as the juncture element and the secondary plate as the isolated body. While the secondary plate is idealized by a rigid body mass, the fuselage panel and the isolator are simulated considering their elastic dynamic behavior.

One approach for the derivation of an admittance model that considers the elastic dynamic behavior of the body is based on the principle of the modal superposition or the influence of single mode shapes [1], according to the following expression.

$$\frac{v_l(s)}{f_k(s)} = G_{lk}(s) = \sum_{i=1}^{j} \frac{\phi_{li}\ \phi_{ki}}{s^2 + 2\nu_i\ \omega_{0i}\ s + \omega_{0i}^2} \tag{6}$$

Therein the admittance G_{lk}, which relates the velocity of the point l to force f applied to the point k, is calculated by the sum of the admittances of each single mode. Thus, the single admittance of the i^{th} mode considers eigenvector components ϕ_{li}, ϕ_{ki} related to points l and k, the modal damping factor ν_i and the eigenvalue ω_{0i}.

The modal superposition leads to the state-space model, as described in Eq. (7).

$$\begin{bmatrix} \dot{\vec{x}}(t) \\ \ddot{\vec{x}}(t) \end{bmatrix} = \begin{bmatrix} \underline{0} & \underline{I} \\ diag(\omega_{0i}^2) & diag(2\nu_i\ \omega_{0i}) \end{bmatrix} \cdot \begin{bmatrix} \vec{x}(t) \\ \dot{\vec{x}}(t) \end{bmatrix} + \begin{bmatrix} \underline{\phi}^T \end{bmatrix} \begin{bmatrix} \vec{f}_{\text{Pn}}(t) \end{bmatrix} \tag{7}$$

$$\begin{bmatrix} \vec{v}_{\text{Pn}}(t) \end{bmatrix} = \begin{bmatrix} \underline{0} & \underline{\phi}^T \end{bmatrix} \cdot \begin{bmatrix} \vec{x}(t) \\ \dot{\vec{x}}(t) \end{bmatrix} + \begin{bmatrix} \underline{0} \end{bmatrix} \begin{bmatrix} \vec{f}_{\text{Pn}}(t) \end{bmatrix}$$

In the above expression, the input and output points P_{n} are placed on the flexible structure considered in the system simulation. The state-space model can be derived only on base of modal data derived from i.e. measurement or numerical simulation. Together with the above estimated modal data, the given state-space formulation enables the integration of the dynamic behavior of the fuselage panel into the simulation environment.

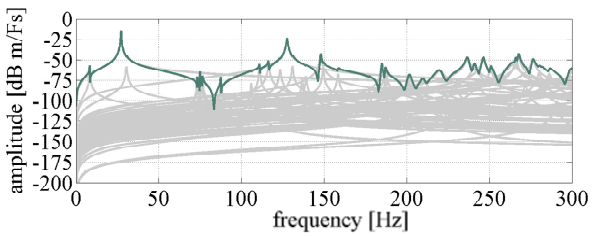

Figure 7: Exemplary point admittance of the excited fuselage panel

By the size of the eigenvector, the model of the panel is reduced to 253 input and output points. As an example, the admittance at one randomly chosen point of the panel is depicted in Figure 7.

The modeling of the isolator can be carried out in a similar way. However, high stiffness elements have to be included additionally, since the isolator has to be modeled as impedance. Furthermore, the electro-mechanical coupling is included by the transfer behavior of the electrical actuator voltage to the equivalent mechanical force. The complete isolator model is schematized in Figure 8. By an automated analytical optimization, the geometrical parameters of the isolator are calculated [4]. The resulting eigenfrequencies are estimated to $f_{e,1} = 36{,}3$ Hz and $f_{e,2} = 1048$ Hz and therefore fit the goal parameters. The voltage to force transduction factor is estimated to a maximal value of $k_T = 0{,}19$ N/V.

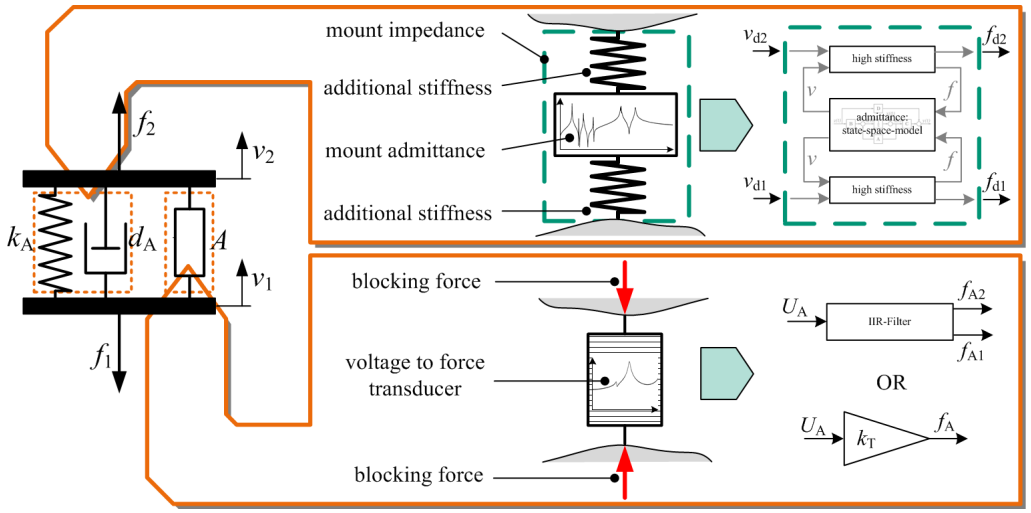

Figure 8: Modeling scheme of the isolator

The purely mechanical part is described by the state-space model and the modal data. The simulated or measured voltage to force transduction can be estimated by an IIR-Filter or a simple gain factor k_T. While a gain factor is sufficient in the case of an approximately frequency-constant transduction behavior, the IIR-filter enables the simulation of high order dynamic influences.

Finally the single components are assembled to the shunted system as shown in Figure 6(b). The impedance of the shunted isolator combines the impedances of the mechanical system Y_{me} and the electrical system Y_{el}.

3.3 Simulation results

Based on the excitation scenario as described on topic 1.2, one point of the fuselage panel is excited by a force signal according to Figure 6(b). As simulation results, the velocity spectra of the excited panel and the isolated plate are depicted for different shunt configurations in Figure 9. It can be seen, that in all cases a broad banded isolation that increases to higher frequencies is achieved above approx. 50 Hz.

In Figure 9(a), the result of the isolation without shunted circuit is shown. Both the resonance amplification at approx. 35 Hz and the first harmonic at 50 Hz are clearly visible in

the velocity spectrum of the plate that is to be isolated. Using an *RL*-shunt that is optimized to 35 Hz, the resonance amplification can be reduced, as can be seen in Figure 9(b). Figure 9(c) illustrates the comparison to an *RL*-shunt which is tuned to the harmonic excitation at 50 Hz, thereby resulting in a reduction of the harmonic amplitude. Thus, the simulation results show the principle usage of the shunted isolator for an improved passive isolation of the idealized plane fuselage demonstrator setup.

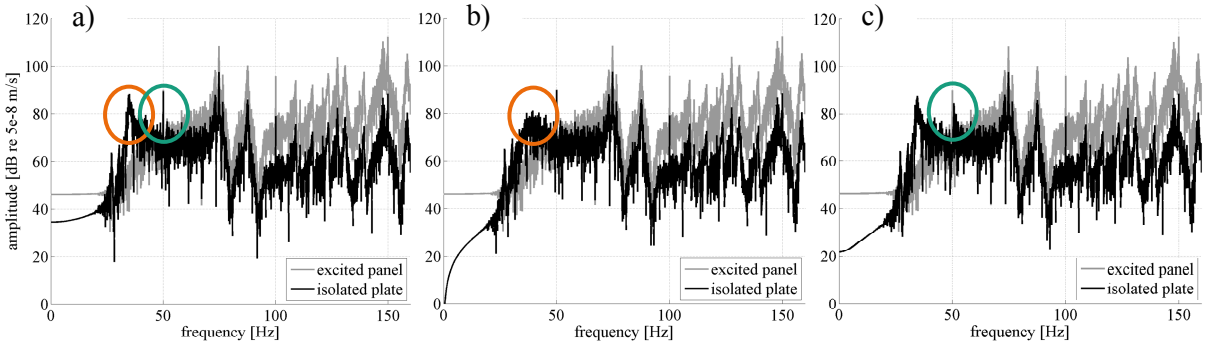

Figure 9: Simulated comparison between the excited panel and the isolated plate
a) Isolation without shunt
b) Isolation with optimized *RL*-shunt in the resonance frequency of the isolator (35 Hz)
c) Isolation with L-shunt, tuned to the first harmonic excitation frequency (50 Hz)

4 LAYOUT OF THE RL-SHUNT

As described above, the classical *RL*-shunt consists of the piezoelectric element with a capacitive behavior, a passive electrical resistor and an inductance. In order to absorb the first eigenfrequency at 35 Hz of the vibration isolator, the electrical eigenfrequency of the shunt has to be tuned to match this frequency. The electrical eigenfrequency of the shunted system is defined by Eq. (8).

$$\omega_e = \sqrt{\frac{1}{LC_{pi}^S}} \tag{8}$$

In Eq. (8), C_{pi}^S is the inherent capacitance of the clamped piezoelectric element [9]. The combined capacitance of the piezoelectric transducers is 160 nF. With ω_e being 219.9 rad/s, the optimal inductance is calculated by solving Eq. (8) for *L*, leading to a value of 129.2 H, which is realized by a synthetic inductor. The circuit diagram and the finally realized SMD board are shown in Figure 10.

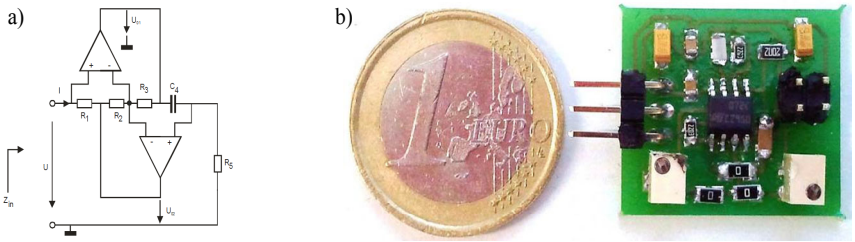

Figure 10: Realization of the synthetic inductor
a) Circuit diagram of the inductor (Mayer, et al., 2001)
b) Picture of the SMD circuit board

Since the tuning of the shunt to the structural eigenfrequency is an essential part in order to obtain good damping values, the synthetic inductor L can be adjusted by a potentiometer. This allows values between 0,2 H and 220 H.

Furthermore, another potentiometer in series to the piezoelectric transducer and the synthetic inductor is integrated to continously change the damping values of the shunted system. The optimal resistance to achive best damping values can be calculated by Eq. (9), given amongst others by [17].

$$R = \frac{\sqrt{2}K_{ij}}{C_{pi}^{S}(1+K_{ij}^{2})} \tag{9}$$

K_{ij} describes the generalized electromechanical coupling coefficient [9].

5 MEASUREMENT RESULTS OF A TEST SETUP

A first test setup, as illustrated in Figure 11, is implemented to assure both the accuracy of the simulation model and the usability of the hardware realization of the shunted isolator.

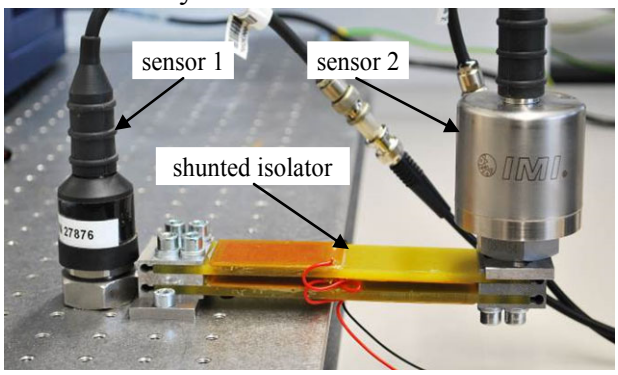

Figure 11: Test setup of the shunted isolator system

While the basement (excited part) is excited by a random signal, the transmissibility from the basement to the free oscillating side of the isolator (isolated part) is measured by the shown acceleration sensors. The accelerometer at the isolated part serves as sensor as well as system mass, thus causing a resonance frequency at approximately 35 Hz. The simulation model presented in chapter 3.2 is simplified to the test setup condition, meaning that a rigid body is considered as exited part.

Figure 12(a) shows the simulation and Figure 12(b) shows the measurement results of the transmissibility of the isolator according to the test setup and for different shunt configurations. The measurement shows the predicted behavior of the shunted isolator. A tuned *L*-shunt behaves similar to a mechanical vibration absorber, thus causing a new resonance frequency and a zero point at the resonance frequency of the system. Introducing a resistor, the *RL*-shunt adds a damping effect which can be easily tuned to an optimized value. The result is a reduction of the resonance frequency without the loss of isolation at higher frequencies. An analysis shows that the measured behavior can be predicted sufficiently well by the presented simulation model. Therefore, the optimization procedure and the simulation model are usable for preliminary design tasks.

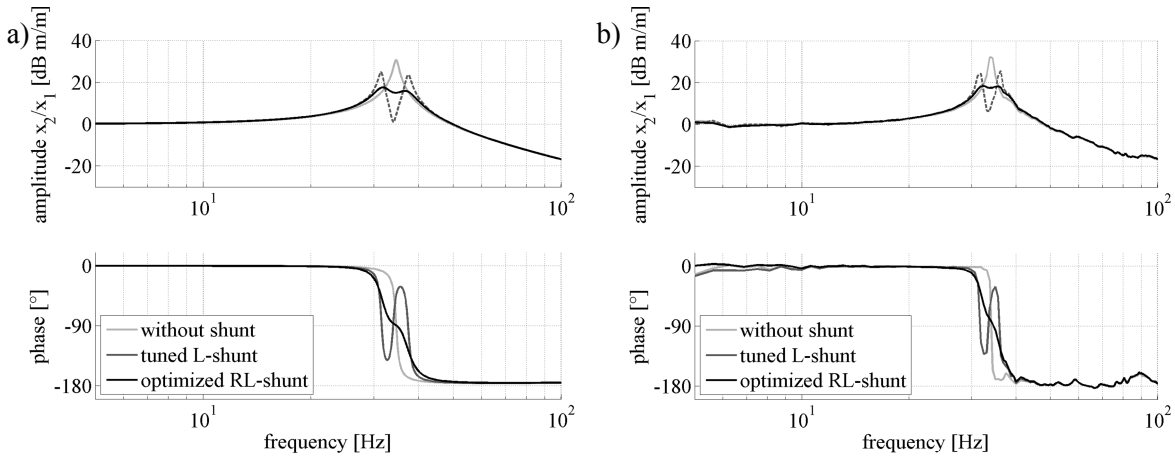

Figure 12: Transmissibility curves of the shunted isolator in a test setup
a) Simulation
b) Measurement

6 EXPERIMENTAL RESULTS OF THE VIBRATION ISOLATION FROM THE EXCITED AIRCRAFT PANEL

In the demonstrator setup, two shunted isolators are positioned between the idealized aircraft panel and the mass to be isolated. Figure 13 illustrates the measurement setup including the used acceleration sensors.

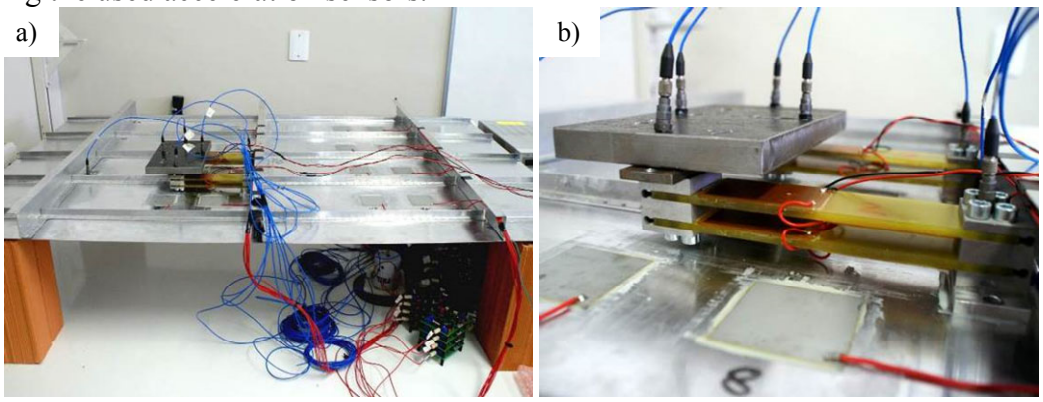

Figure 13: Measurement setup
a) Aircraft panel with attached shunted isolator
b) Attached pair of shunted isolators with isolated mass

The measurement result of the passive isolation effect is depicted in Figure 14(a), while the panel is excited by a random shaker signal. Towards higher frequencies, the acceleration of the isolated side is increasingly lower in comparison to the excited panel. At approximated 37 Hz, an amplification of the acceleration occurs due to the isolation system's resonance. At figure 14(b) the acceleration of the isolated side with and without shunt is compared. With the activated shunt, the acceleration amplification in the resonance frequency is reduced significantly.

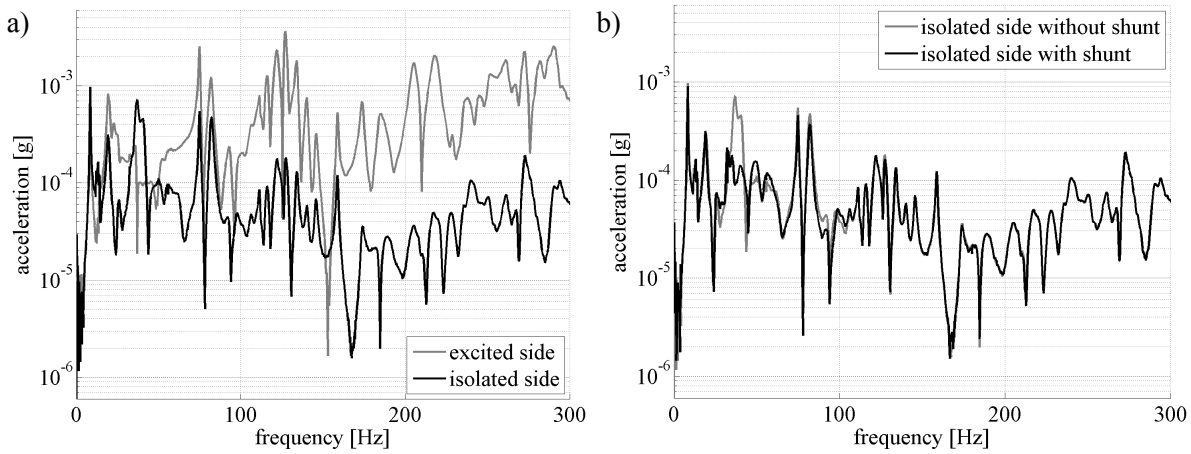

Figure 14: Measured acceleration spectra
a) Comparison between the excited and isolated side
b) Comparison between the isolated side without and with shunt (optimized to 37 Hz)

7 CONCLUSIONS

This paper shows the concept, the modeling and the design of a shunted piezoelectric isolator. Thereby, the usefulness of the system in order to positively influence the transmission behavior of an idealized isolation system is shown by simulation and measurement. By using a design methodology and the presented simulation model, the required dimensions of the isolator can be effectively estimated. In comparison to measurement results, the quality of the simulation model is proven. Simulation and measurement results of a holistic model, in which an elastic behavior of the base structure is included, show a promising vibration reduction effect of the excited fuselage demonstrator. In a next step, a more integrable shunted isolator is to be set up.

8 ACKNOWLEDGEMENTS

The research presented in this paper was performed in the framework of the projects FuMaxSIs (Federal Ministry of Education and Research, Germany), LOEWE AdRIA (State of Hesse, Germany), the PROBRAL program of the DAAD (Germany). The financial support by these projects is gratefully acknowledged. The Brazilian authors acknowledge the CAPES/ Probral, CNPq and INCT for the financial support received during this work.

9 REFERENCES

[1] Bartel, T., Atzrodt, H., Herold S. and Melz, T. *Modeling of an Active Mounted Plate by means of the Superposition of a Rigid Body and an Elastic Model*. In *Proceedings of the International Conference on Noise and Vibration Engineering - ISMA*, (2010), Leuven, Belgium.

[2] Bartel, T., Baghaie Yazdi, M., Melz, T. and Tarle P. *Optimization and measurement of a flexible sensitive sensor design*. In *Proceedings of the Conference on Smart Structures and Materials - SMART*, (2011), Saarbrücken, Germany.

[3] Bartel, T., Koch, M., Matthias, M. and Tarle P. *Simulation, development, and testing of a triaxial vibration isolation platform*. In *Proceedings of the International Conference on Noise and Vibration Engineering - ISMA*, (2012), pp. 151-162, Leuven, Belgium.

[4] Bartel, T., Heuss, O., Mayer, D., Melz, T., Scinocca, F., Nabarrete, A. and Goes, L.C.S. *Design of a shunted isolator for reduction of the vibration transmission of a plane fuselage*. In: *22nd International Congress of Mechanical Engineering*, (2013), Brazil.

[5] Bastaits, R., Mokrani, B. and Preumont, A. *Control-Structure Interaction in Active Optics of Future Large Segmented Mirrors*. In *Proceedings of the International Conference on Noise and Vibration Engineering - ISMA*, (2010), Leuven, Belgium.

[6] De Marneffe, B., Horodinca, M. and Preumont A. *Vibration isolation via shunted electromagnetic transducers*. In *Proceedings of the International Conference on Noise and Vibration Engineering - ISMA*, (2008), Leuven, Belgium.

[7] Fuller, C. R., Elliott, S. J. and Nelson, P.A. Active Control of Vibration. Academic Press., (1997).

[8] Hagedorn, P. and DasGupta, A. Vibration and Waves in Continuous Mechanical Systems. John Wiley & Sons Ltd, (2007), West Sussex, England.

[9] Hagood, N. W., von Flotov, A. Damping of Structural Vibrations with Piezoelectric Materials and Passive Electrical Networks. *Journal of Sound and Vibration*, (1991), 146(2), pages 243-268.

[10] Herold, S., Atzrodt, H., Mayer, D. and Thomaier, M. *Modeling Approaches for Active Systems*. In *Proceedings of the SPIE, Symposium Smart Structures and Materials and NDE for Health Monitoring and Diagnostics*, (2006), No. 6173-24, San Diego, USA.

[11] Hidalgo, I. L., Nabarrete, A. and Santos M. Structure-borne transmissibility evaluation through modeling and analysis of aircraft vibration dampers. *Journal of Aerospace Technology and Management*, (2011), Vol. 3, No. 2, pp. 147-158.

[12] Konstanzer, P., Grünwalder, M., Jänker, P. and Storm, S. *Aircraft interior noise reduction through a piezo tunable vibration absorber system*. In *Proceedings of the 25th International Congress of the Aeronautical Sciences*, (2006), Hamburg, Germany.

[13] Lo, W., Hinote, G. and Shih, C. *Identification of structural operating modes for aircraft cabin noise reduction*. In *Proceedings of IMAC-XX: A Conference on Structural Dynamics*, (2002), Los Angeles, USA.

[14] Mayer, D., Linz, Ch. and Krajenski, V. *SynthetischeInduktivitätenfür die semi-passive Dämpfung*. *5. MagdeburgerMaschinenbau-Tage – Entwicklungsmethoden und EntwicklungsprozesseimMaschinenbau*, (2001), Magdeburg

[15] Preumont A. *Vibration Control of Active Structures: An Introduction*. Springer, 3rdedition,(2011).

[16] Schmidt, M., Atzrodt, H., Sabirin, C. R., Rue, de, G.J. and Melz, T. *Comparative operational modal analysis: Application of a semi-active vibration absorber to a manufacturing machine*. In: *Proceedings of the 4th International Operational Modal Analysis Conference (IOMAC*), (2011), Istanbul, Turkey.

[17] Viana, F. and Valder, S. *Multimodal Vibration Damping Through Piezoelectric Patches and Optimal Resonant Shunt Circuits.* In *J. of the Braz. Soc. of Mech. Sci. & Eng.* 3, (2006), pages 293–310.